Journal of Applied Polymer Science

Cure Kinetics of an Acrylated Epoxidized Hemp Oil-Based Bioresin System

Gaston Francucci,[1,2] Francisco Cardona,[2] Nathan W. Manthey[2]

[1]Composite Materials Group, Research Institute of Material Science and Technology (INTEMA-CONICET), Materials Engineering Department, Engineering Faculty, National University of Mar del Plata. J. B. Justo 4302, B7608FDQ, Mar del Plata, Argentina

[2]Center of Excellence in Engineered Fibre Composites (CEEFC), Faculty of Engineering and Surveying University of Southern Queensland, Toowoomba, Queensland 4350, Australia

Correspondence to: G. Francucci (E-mail: gfrancucci@fi.mdp.edu.ar)

ABSTRACT: In this work, the cure kinetics of a novel acrylated epoxidized hemp oil (AEHO)-based bioresin was investigated for the first time by differential scanning calorimetry (DSC) using both isothermal and nonisothermal conditions. This new bioresin was synthesized by the acrylation of a previously epoxidized hemp oil (EHO) bioresin. The curing of the AEHO bioresin showed an autocatalytic behavior with the vitrification phenomenon preventing the conversion reaching unity for all the temperatures studied. It was found that the curing behavior can be modeled with high accuracy using a modified Kamal autocatalytic model that takes into account the vitrification phenomenon. Dynamic activation energies were determined from the Kissinger and Ozawa–Flynn–Wall methods, resulting in 58.87 and 62.02 kJmol^{-1}, respectively. In addition, activation energies associated with the autocatalytic model constants, k_1 and k_2, were established to be equal to 58.94 and 45.32 kJmol^{-1}, respectively. © 2012 Wiley Periodicals, Inc. J. Appl. Polym. Sci. 128: 2030–2037, 2013

KEYWORDS: biopolymers and renewable polymers; differential scanning calorimetry; kinetics; thermosets; resins

Received 1 May 2012; accepted 22 July 2012; published online 13 August 2012
DOI: 10.1002/app.38380

INTRODUCTION

Nowadays, the increasing environmental pollution and the depletion of nonrenewable resources have led industry and academia to focus research on the development of materials that are environmentally friendly and/or made from renewable resources. In this context, biocomposites are being created using natural fibers in conjunction with bioresin matrices. Thermoset bioresins are a valid alternative to their commercial equivalents such as epoxy, vinylester, polyester and phenolic resins. These thermoset bioresins are produced mainly from natural triglyceride oils which in turn are obtained from plants/vegetables. Although most of thermoset bioresins are nonbiodegradable,[1] they are an attractive alternative to petroleum-based resins because they are inexpensive, have structural properties similar to their synthetic equivalents and are produced from natural, renewable resources offering sustainability in addition to low environmental impact. Most bioresins are made from chemically modified triglycerides, which are the main component of plant oils. Wool and Khot[1] reviewed the numerous ways of chemically modifying the unsaturated sites on the fatty acids from the triglyceride oils.

The study of the cure kinetics of resins is of major importance, because most of their physical properties and processability largely depend on the reaction rate and degree of cure which in turn depend on the curing conditions (time and temperature). Knowledge about the cure kinetics allows determining the optimal processing parameters and the most suitable curing cycle that assures the highest productivity rate along with satisfactory product properties. Numerous cure kinetics studies can be found in literature on many synthetic thermoset systems.[2–15] However, not much information about the cure kinetics of vegetable oil-based resin systems can be found in the literature. In the last two decades researchers have studied the cure kinetics of typical vegetable oil-based bioresins such as epoxidized soybean oil (ESO),[16] epoxidized methyl soyate (EMS),[17] epoxidized allyl soyate (EAS),[18] soybean oil-styrene-DVB thermosetting copolymers,[19] epoxidized castor oil (ECO),[20] and epoxidized linseed oil (ELO).[21]

Industrial hemp oil also has a significant potential as a bioresin feedstock because of its fatty acid profile. Manthey et al.[22,23] reported for the first time the cure kinetics of an epoxidized hemp oil (EHO)-based bioresin. The authors obtained a good agreement of the model predictions with the experimental values by modifying Kamal's autocatalytic isothermal model to account for the diffusion effects post vitrification. Although the EHO bioresin is by itself suitable as a polymeric matrix for

biocomposites, further modifications can be made on its chemical structure to modify its functionality. Reaction of epoxy functional triglyceride with acrylic acid incorporates acrylate chemical groups onto the triglyceride, attaching vinyl functionalities to its structure.[1,24] After this modification, an acrylated epoxidized hemp oil (AEHO)-based bioresin is obtained. This new monomer can be blended with a reactive monomer such as styrene and cured by the typical free radical polymerization mechanism. The addition of the reactive monomer (styrene), also lowers the resin viscosity making it suitable for most liquid composite processing techniques.[25] Therefore, AEHO-based resins are analogous to the synthetic vinyl esters (VE) and unsaturated polyester (UPE) resins.

The aim of this investigation is to model the cure behavior of AEHO-based bioresins which, to our knowledge, has not been previously studied and reported. Dynamic and isothermal cure kinetics using differential scanning calorimetry (DSC) was investigated and the determination of activation energies and modeling of the cure behavior is discussed throughout this article. The results showed that this resin displays an autocatalytic behavior controlled by diffusion because of the vitrification phenomenon. Consequently, prediction of the curing behavior could be obtained with satisfactory precision using an autocatalytic model modified to account for vitrification.

EXPERIMENTAL

Materials

In this work, cold pressed raw industrial hemp oil supplied by Ecofibre (Maleny, Queensland, Australia) was used. The fatty profile of the raw industrial hemp oil is shown in Table I. The viscosity of the bioresin after the acrylation process was measured at room temperature (25°C) by means of a Brookfield DV–II+ viscometer, obtaining a value of 20550 CP. This viscosity is too high for most composite processing techniques. Therefore, 33% by weight of styrene was added to the bioresin to decrease its viscosity and make it suitable for manufacturing composite parts by the traditional composite processing techniques. The viscosity after the styrene addition was 358 CP at room temperature. Afterward, the promoter (accelerator N2-51 P from Axon Nobel) was incorporated to the mixture (0.25% by weight). A 40% MEKP-based catalyst (from FGI Australia, Company) was added (4% by weight) and stirred thoroughly for a couple of minutes before every DSC run. Styrene is a fully miscible coreactant added to decrease the resin viscosity. The promoter is added to activate the MEEKP-based catalyst to initiate the free radical polymerization of the double bonds present in the blend of styrene and AEHO-based bioresin.

Table I. Fatty Profile of the Raw Industrial Hemp Oil used in this Study

Fatty acid	%
Palmitic	6.0
Stearic	2.0
Oleic	12.0
Linoleic	57.0
Linolenic	20.7
Other	2.3

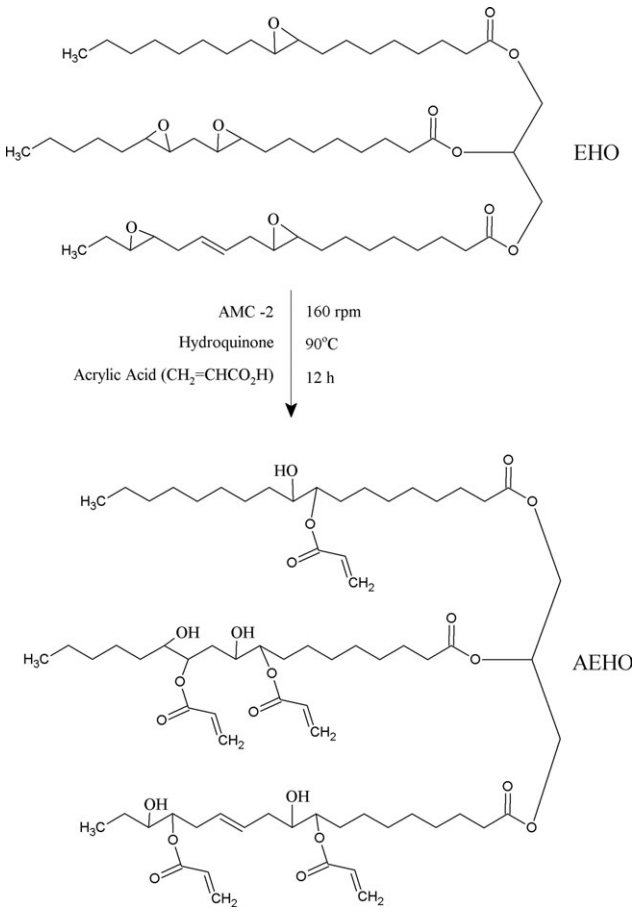

Figure 1. *In situ* acrylation of epoxidized hemp oil.

Synthesis of Acrylated Epoxidized Hemp Oil

AEHO was obtained by the acrylation of the EHO obtained in previous works.[22,23] A solution of EHO, hydroquinone inhibitor (0.0033 g mL^{-1} of EHO + acrylic acid) and AMC-2 catalyst (1.75% by weight of EHO + acrylic acid) were added to a Mettler Toledo LabMax automatic reactor. The reactor comprised of a 4 -L four-necked reaction vessel equipped with a mechanical "ship anchor" stirrer and thermometer. Stirring was initiated and the reactor temperature was increased until the mixture reached 50°C. The mixture was left at that temperature for 30 min and then the acrylic acid (ACROS Organics) was added in a molar ratio of 1.1 moles *per* mol of epoxy groups. The exothermic reaction increased the temperature of the mixture rapidly, thus the reactor was set to maintain a constant temperature of 90°C. The reaction was then performed at the mentioned temperature, stirring the mixture at 160 rpm over a period of 12 h. The reaction evolution was monitored by periodic titulation of the AHEO/acrylic acid mixture using sodium hydroxide and phenolphthalein as an acid–base indicator. The reaction was considered to be complete when no further changes could be seen in the amount of sodium hydroxide used to neutralize the resin. Figure 1 shows schematically the *in situ* acrylation of the epoxidized hemp oil.

Curing Kinetics Using DSC

A calibrated TA Instruments DSC Q100 with Universal Analysis 2000 version 3.9 A software was used for the dynamic and isothermal analysis. Dry nitrogen gas at 80 mLmin^{-1} was used during the experiments to purge the DSC cell. Samples between 10 and 15 mg were enclosed in hermetic aluminum DSC sample pans. Dynamic scans were performed at four different heating rates 5, 10, 15, and 20°C min^{-1} from 10 to 250°C. The samples were then cooled to 10°C at a rate of 10°C min^{-1}. To complete the heat-cool-heat cycle, the samples were reheated to 250°C to confirm the nonexistence of any residual curing. Isothermal scans were performed at five different temperatures 50, 65, 70, 75, and 80°C, determined from the dynamic DSC data. The isothermal scans were deemed to be complete when the thermograms leveled off to a predetermined baseline. After the isothermal runs, the samples were reheated at 10°C min^{-1} from 10 to 250°C to determine the residual heat of reaction. To verify consistency of data, two runs were performed for every condition.

DSC Analysis Theory

Both, dynamic and isothermal methods can be used to analyze the cure kinetics of thermosetting polymers. Dynamic kinetic methods use a constant heating rate and are not quantitatively applicable to autocatalytic systems. Isothermal kinetic methods use a constant temperature and are able to be applied to both autocatalytic and nth order.[22]

DSC equipment measures the heat generated by reactions. The main assumption used to study the curing kinetics by this technique is that the heat flow, dH/dt, is proportional to the reaction rate, $d\alpha/dt$. The degree of cure, α, is proportional to the heat generated during the exothermic cure reaction and can be calculated by eq. (1) where, ΔH_t is the accumulative heat of reaction given from DSC scans up to a certain time, t, and ΔH_{total} is the total reaction heat. The accumulative heat of reaction is obtained by integrating the exothermic peak of the DSC curve. In the same way, the residual heat of reaction is obtained by integrating in time the whole peak shown in the DSC runs performed at the reheating stage. The total reaction heat is the sum of the isothermal heat of reaction plus the residual heat of reactions.[26,27] For modeling purposes, it is adequate to consider the value of ΔH_{total} to be the averaged value of the heats of reactions obtained from the dynamic runs at different heating rates.[13] The reaction rate can be calculated from eq. (2).

$$\alpha = \frac{\Delta H_t}{\Delta H_{\text{total}}} \tag{1}$$

$$\frac{d\alpha}{dt} = \frac{(dH/dt)}{\Delta H_{\text{total}}} \tag{2}$$

Isothermal Cure Kinetics

From eqs. (1) and (2), kinetic models capable of predicting the curing behavior of thermosetting polymers can be developed. Except for the models derived by Horie et al.[28] and Sourour and Kamal,[29] phenomenological models employed by many investigators were purely empirical.[26] The general form of the rate equation, in absence of diffusion control, that is used in all the kinetic models is shown in eq. (3), where $k(T)$ is the reaction rate constant, and $f(\alpha)$ is the function that is dependent on α. The reaction rate constant is an Arrhenius function of temperature, as shown in eq. (4), where A is the pre-exponential factor, E_a is the activation energy (the difference in enthalpies of the transition state and the initial state), R is the universal gas constant, and T is the absolute temperature.

$$\frac{d\alpha}{dt} = k(T)f(\alpha) \tag{3}$$

$$k(T)_i = A_i e^{-\frac{E_a}{RT}} \tag{4}$$

Many different expressions have been proposed for the function $f(\alpha)$, being the simplest the nth order equation, eq. (5), where k is the reaction rate constant and n is the order of reaction.

$$\frac{d\alpha}{dt} = k(1-\alpha)^n \tag{5}$$

Typically, the form of $f(\alpha)$ used for autocatalytic reactions is the one shown in eq. (6) if the initial reaction rate is zero, or the one show in eq. (7) if the initial reaction rate is not zero:

$$\frac{d\alpha}{dt} = k\alpha^m(1-\alpha)^n \tag{6}$$

$$\frac{d\alpha}{dt} = (k_1 + k_2\alpha^m)(1-\alpha)^n \tag{7}$$

where k_1 and k_2 are the reaction rate constants and m and n are orders of reaction. In autocatalytic reactions, one of the reaction products is also a catalyst for further reactions.[22] The expression shown in eq. (7) corresponds to Kamal's model which has been successfully applied to many autocatalytic reactions of a diversity of resin systems.[30]

Vitrification usually occurs during the isothermal curing of thermosetting resins. This phenomenon involves a transformation from a liquid or rubber state to a glassy state as a result of an increase in the molecular weight caused by the high degree of polymerization. Near vitrification, the reaction rate decreases drastically and the kinetics are affected by the local viscosity, which in turn depends on the temperature and extent of reaction. As a consequence, the reaction "freezes" and the degree of reaction reaches a maximum value, $\alpha_{\text{max}} < 1$, for a given cure temperature. Therefore, the previously mentioned phenomenological models can be modified to account for vitrification, by adding a new term that is a function of α_{max}.[27,31,32]

$$\frac{d\alpha}{dt} = k(T)g(\alpha_{\text{max}})f(\alpha) \tag{8}$$

Different expressions were proposed for the function $g(\alpha_{\text{max}})$. Some examples are shown in eq. (9)[31,33] and eq. (10),[34,35] where x and C are new adjustable parameters.

$$g(\alpha_{\text{max}}) = \left(\frac{\alpha_{\text{max}} - \alpha}{\alpha_{\text{max}}}\right)^x \tag{9}$$

$$g(\alpha_{\text{max}}) = \frac{1}{1 + e^{C(\alpha - \alpha_{\text{max}})}} \tag{10}$$

In addition, Kamal's model can be modified to account for the vitrification phenomenon, incorporating an α_{max} term to prevent the conversion exceeding the degree of cure associated with the vitrification[22]:

$$\frac{d\alpha}{dt} = (k_1 + k_2\alpha^m)(\alpha_{max} - \alpha)^n \quad (11)$$

Dynamic DSC Measurements

Dynamic DSC measurements overcome some of the drawbacks of isothermal DSC analysis, such as being time-consuming[36] inaccuracy of the initial cure data caused when the sample must be heated quickly to the chosen cure temperature[37] and data errors caused by the premature reaction start during the initial heating ramp up to the cure temperature. Some authors have found the kinetic parameters estimated from nonisothermal DSC measurements to be different from the ones obtained through isothermal DSC measurements.[38,39] On the other hand, other authors have found similar values for the kinetic parameters evaluated by both thechniques.[40,41]

Two dynamic kinetic models based on multiple heating rates that are useful in determining the activation energy of the curing reaction have been proposed by Kissinger[15] and Ozawa–Flynn–Wall.[42,43] Both methods are independent of the reaction order and therefore simplify the complexity of the curing reaction. The activation energy can be estimated using the former method from the slope of the plot $\ln(q/T_m^2)$ vs. $1/T_m$, [eq. (12)], or with the Ozawa–Flynn–Wall method from the slope of the curve *log q* vs. $1/T_m$ [eq. (13)], where q is the heating rate and T_m is the peak temperature.

$$\frac{d\left[\ln\left(q/T_m^2\right)\right]}{d(1/T_m)} = -\frac{E_a}{R} \quad (12)$$

$$\log q = \log\left(\frac{AE_a}{g(\alpha)}\right) - 2.315 - \frac{0.4567E_a}{RT_m} \quad (13)$$

RESULTS AND DISCUSSION

Dynamic DSC Analysis

The curves obtained from the dynamic DSC runs at different heating rates are shown in Figure 2. It can be seen that both peak temperature and heat of reaction increased with increased heating rates, showing the same trend observed previously for the EHO/TETA,[22] EHO/TETA/IPD,[23] and epoxy[44–46] systems. On the other hand, many authors did not find a clear trend regarding epoxy,[47,48] polyester and vinyl ester[26,49] systems. Therefore, considering that in our results as well as the mentioned cases the difference between the heat of reaction values was <5%, it can be concluded that the dispersion of the data is in the order of the experimental and data processing error and no correlation can be established between the heat of reaction and the heating rate, as suggested by Kenny and Trivisano.[13] Table II presents the values of peak temperatures and heat of reactions calculated from the dynamic DSC curves.

Plots of *ln* (q/T_m^2) vs. $1000/T_m$, and *log q* vs. $1000/T_m$ corresponding to the Kissinger and Ozawa–Flynn–Wall methods respectively, are shown in Figure 3. Both models seem to be valid given that the degree of linearity found in the plots was very high. The activation energy found by applying the Kissinger model was 58.87 kJ mol^{-1}, while the Ozawa–Flynn–Wall model gave a slightly higher activation energy, of 62.02 kJ mol^{-1}. These results are consistent with other researchers' findings for epoxy,[2,44,48] epoxidized linseed oil,[21] and epoxidized hemp oil,[22,23] who also found activation energies from the Ozawa–Flynn–Wall model to be marginally higher than the values determined by the Kissinger model.

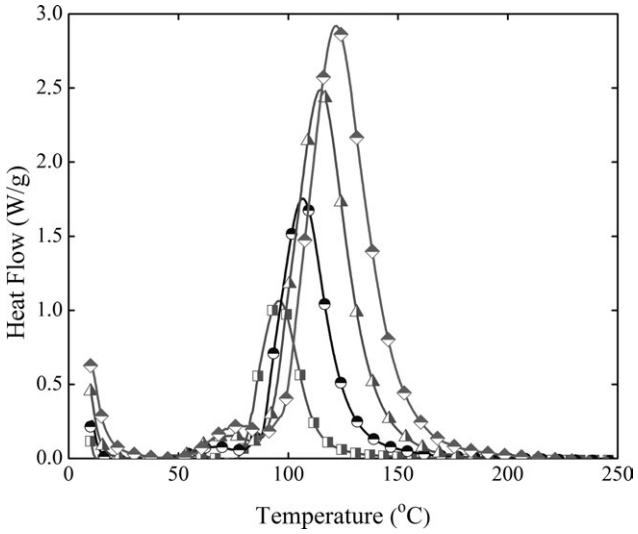

Figure 2. Dynamic DSC curves of AEHO-based bio-resin at 5°C min^{-1} (—■—), 10°C min^{-1} (—●—), 15°C min^{-1} (—▲—), and 20°C min^{-1} (—◆—).

Isothermal Kinetics Analysis

Isothermal reaction rate profiles obtained for the different applied cure temperatures are shown in Figure 4. A significant induction time (the period of time which there is no reaction) can be seen for the 50°C isothermal curing condition. As expected, the higher the temperature, the faster the overall reaction. In addition, the onset of reaction and the maximum reaction rate occur earlier as the cure temperature is increased. Table III presents the values of the induction time, t_z, and the time at the maximum reaction rate, t_m, for all the temperatures studied.

Values of the reaction rate $d\alpha/dt$ plotted in Figure 4 was calculated by dividing the original DSC signal, dH/dt, by the averaged total heat of reaction obtained from the dynamic DSC runs (see Table II), as stated in eq. (2). The total heat of

Table II. Heats of Reaction and Peak Temperatures at Different Heating Rates

q (°C min^{-1})	ΔH_{total} (J g^{-1})	T_m (°C)
5	317	96.06
10	317.1	106.53
15	320.2	114.75
20	334.9	121.9
Avg. ΔH_{total} (J g^{-1})	322.3	

Applied Polymer SCIENCE

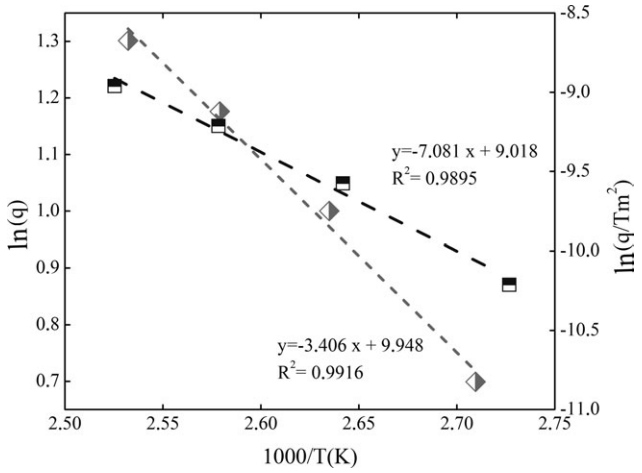

Figure 3. Plot to determine Kissinger (■) and Ozawa–Flynn–Wall (◑) activation energies.

reaction developed in each isothermal experiment, H_T, can be obtained by the integral of the peaks of the original DSC plots, *dH/dt* vs. *time*. In the same way, the residual heat, H_R, is obtained by the integration of the peak observed in the reheating stage performed after each isothermal run. The sum of H_T and H_R gives the total heat of reaction of the isothermal test, H_{total}. The values of H_T, H_R, H_{total} obtained in the isothermal runs are presented in Table IV. As expected, the residual heat decreased when the cure temperature was increased, showing that the reaction reached higher degrees of conversion when the resin was cured at higher temperatures. The value of H_{total} was not expected to change with the curing temperature, since it comprises of both H_T and H_R. However, an increasing trend was observed with increasing curing temperature in accordance with the findings of Omrani et al.[46] and Kenny and Trivisano.[13] These authors suggested that the inconsistencies found were caused by some inaccuracies associated with the H_{Total} values because they are affected by the sum of the integration errors of

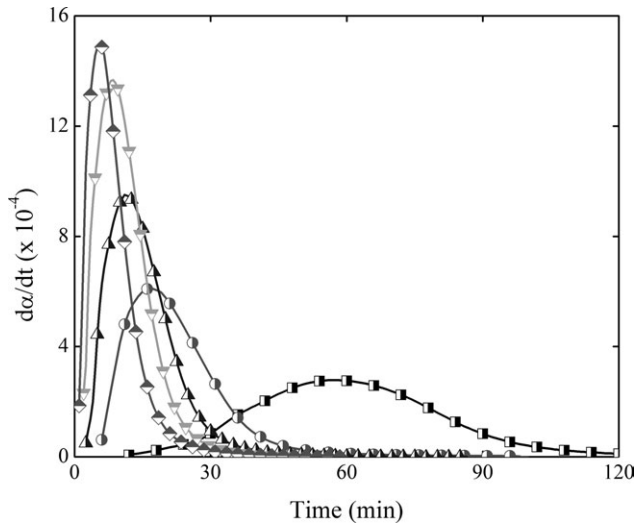

Figure 4. Reaction rate versus time at 50°C (—■—), 65°C (—◑—), 70°C (—◭—), 75°C (—▽—), and 80°C (—◆—).

Table III. t_z and t_m Values for the Isothermal Experiments

Temperature (°C)	t_z (s)	t_m (s)
50	720	3480
65	360	1020
70	150	660
75	120	510
80	60	330

two different peaks and the superposition of the glass transition signal upon the residual reactivity peak.

H_{total} was higher when it was calculated from dynamic runs (see Table II). In addition, its value changed as the curing conditions (both isothermal and nonisothermal) were modified. Therefore, for modeling purposes, the averaged value of H_{total} obtained from the dynamic runs (322.3 J g^{-1}, showed in Table II) was considered as the total heat of reaction, as suggested by Kenny and Trivisano.[13]

The evolution of the degree of cure with time at the curing temperatures used in this study can be seen in Figure 5. As expected, the maximum conversion increased and it was reached faster at higher temperatures of cure. The induction time mentioned previously is also visible in these plots. After this time, the degree of cure increases rapidly within the initial stage of reaction at all temperatures because in this stage the reaction is chemically controlled. At higher α values, diffusion-controlled mechanisms related to the vitrification phenomenon cause the degree of cure to slow down and finally level off to a maximum value, α_{max}, when vitrification is reached.

Figure 6 shows plots of $d\alpha/dt$ as a function of α for the isothermal temperatures. It can be seen that the reaction rate at any given value of α increased as the temperature of cure increased. In addition, the value of $d\alpha/dt$ becomes zero at conversions <1, showing once again that vitrification took place at all the temperatures studied. The behavior of the reaction rate curves suggest an autocatalytic reaction as opposed to simple *n*th order kinetics, because the reaction rate reached a maximum value after the beginning of the cure cycle.

Therefore, Kamal's autocatalytic model, eq. (7), was initially used to model the cure kinetics of the AEHO-based resin. Figure 7 shows the fitting of the experimental data with this model

Table IV. H_T, H_R, H_{total} Obtained in the Isothermal Runs

Cure temperature (°C)	H_T (J g^{-1})	H_R (J g^{-1})	H_{total} Isothermal (J g^{-1})
50	254	19.38	273.38
65	264.3	9.84	274.14
70	273.7	8.69	282.427
75	284.3	8.26	292.56
80	296.6	5.2	301.8

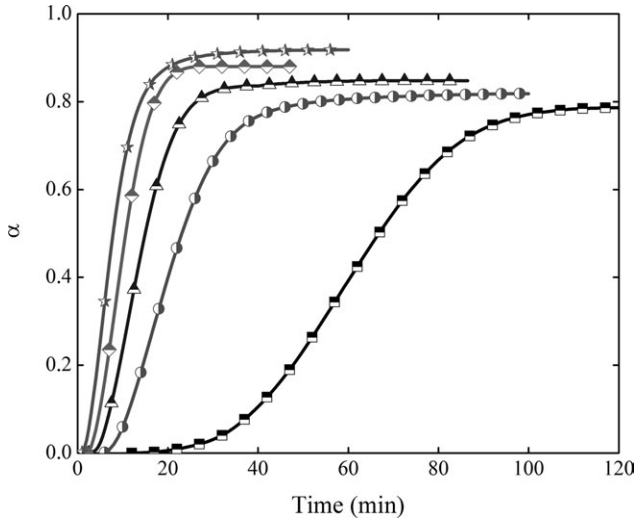

Figure 5. Degree of cure as a function of time for AEHO-based resin at 50°C (—■—), 65°C (—◑—), 70°C (—▲—), 75°C (—◆—), and 80°C (—★—).

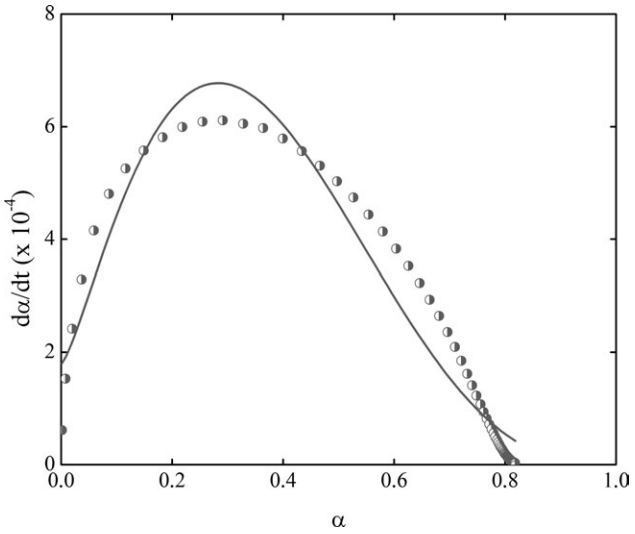

Figure 7. Experimental data (◑) fitted with Kamal's model (——).

for the resin cured at 65°C. It can be seen that the model could not properly fit the experimental data, because it does not account for the vitrification phenomenon that was observed to occur at all the cure temperatures. It should be noted that the same unsatisfactory results were obtained for the other temperatures studied. To improve the model accuracy by considering vitrification, a modified form of Kamal's model, eq. (11), was used. The results of experimental data and model predictions for reaction rate as a function of degree of cure and as a function of time for all the temperatures are shown in Figures 8 and 9, respectively. The agreement of fit is very good for all the temperatures, suggesting that the modified Kamal's autocatalytic model accounting for vitrification can be used to predict the curing behavior of AEHO-based bioresin. The values of the model parameters obtained from the fitting of the experimental curves are presented in Table V. The values of both k_1 and k_2 increased as the temperature increased, and the values of k_2 were higher compared with the values of k_1, suggesting that the reaction may be more influenced by autocatalytic mechanisms than by *n*th order mechanisms. With the exception of the test performed at 80°C, values of *m* were found to decrease when the temperature increased, in accordance to previous findings on the EHO bioresin systems.[22,23] On the other hand, values of *n* did not show a clear trend, as found by other authors,[26,27] although they seem to decrease with the increase of temperature between 65 and 75°C. In a study involving unsaturated polyester resin, it is interesting to note that Vilas et al.[27] found a decreasing trend for *m* and *n* values when experimental data was fitted with traditional autocatalytic models, while they could not obtain any clear trend when an autocatalytic model modified to account for vitrification was used to fit the same data.

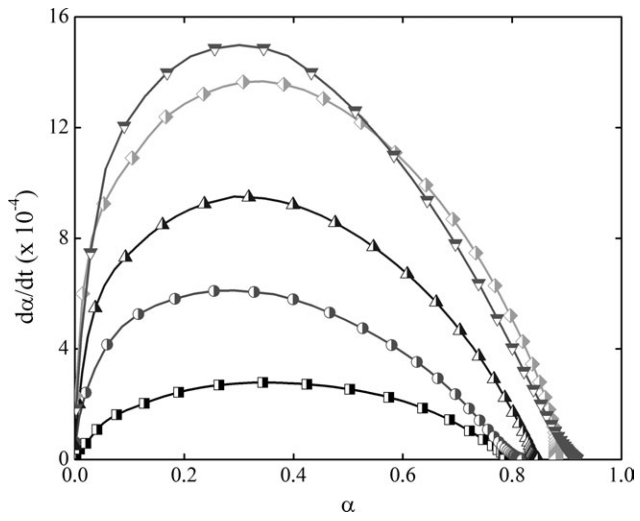

Figure 6. Reaction rate versus degree of cure at 50°C (—■—), 65°C (—◑—), 70°C (—▲—), 75°C (—◆—), and 80°C (—▼—).

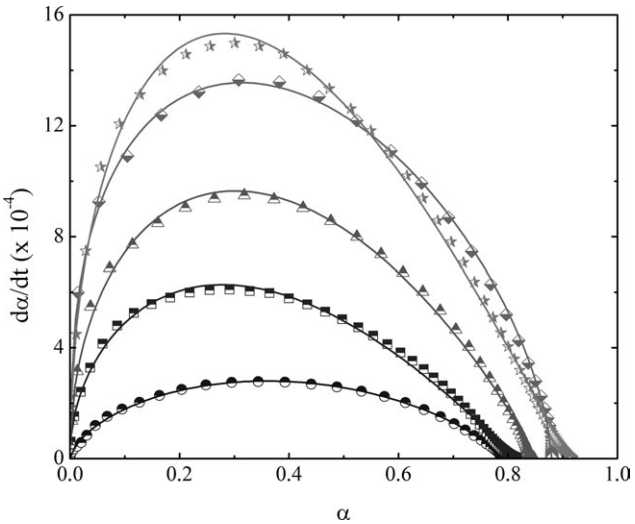

Figure 8. Experimental isothermal DSC data obtained at 50°C (◓), 65°C (■), 70°C (▲), 75°C (◆), and 80°C (★), fitted with the modified Kamal's model accounting for vitrification (solid line).

Applied Polymer SCIENCE

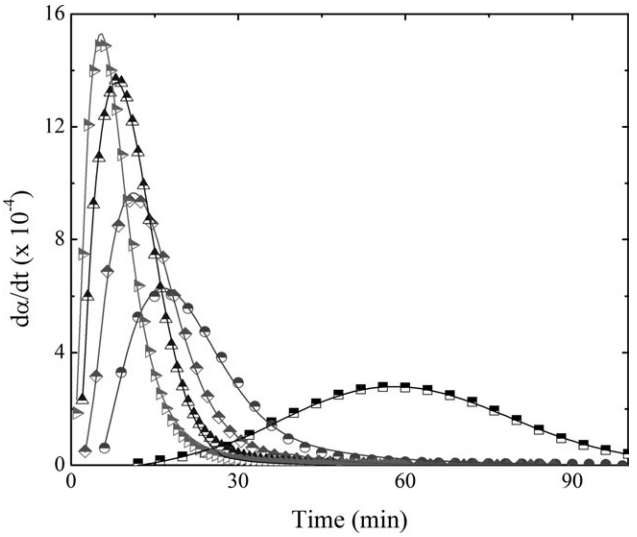

Figure 9. Comparison of experimental data with model predictions (solid line) for reaction rate versus time at 50°C (■),65°C (◓), 70°C (◆), 75°C (▲), and 80°C (▶).

Both reaction rate constants, k_1 and k_2, displayed Arrhenius behavior, as shown in Figures 10 and 11. The activation energies and pre-exponential factors were determined from the gradients and *y*-intercepts of the curves, respectively. The results, summarized in Table VI, showed that the activation energies values obtained from the isothermal DSC experiments were very similar to the values calculated with the Kissinger and Ozawa–Flynn–Wall models applied to the dynamic DSC experimental data.

CONCLUSIONS

The cure behavior of AEHO-based bioresins was investigated by dynamic and isothermal DSC. As expected, the maximum degree of cure increased as the cure temperature increased. The conversion was found to be 0.81 at the lowest temperature used in the DSC tests (50°C) while the highest conversion was 0.92 at the highest cure temperature used (80°C). The AEHO showed an autocatalytic behavior and the vitrification phenomenon prevented the conversion reaching full conversion. Therefore, a modified expression of the autocatalytic Kamal's model that takes into account vitrification was used for the kinetic model. This model fitted with high accuracy the experimental kinetic values for all temperatures, enabling it to be used in further numerical modeling of the curing of AEHO bioresins and biocomposites containing AEHO.

Table V. Autocatalytic Model Parameters

T (°C)	k_1	k_2	*m*	*n*	*m* + *n*	α_{max}
50	8.20 E −06	0.00103	0.658	0.756	1.414	0.811
65	1.50 E −05	0.00233	0.536	1.034	1.570	0.822
70	2.94 E −05	0.00296	0.500	0.889	1.390	0.844
75	3.80 E −05	0.00301	0.380	0.661	1.041	0.896
80	5.00 E −05	0.00471	0.508	1.107	1.615	0.918

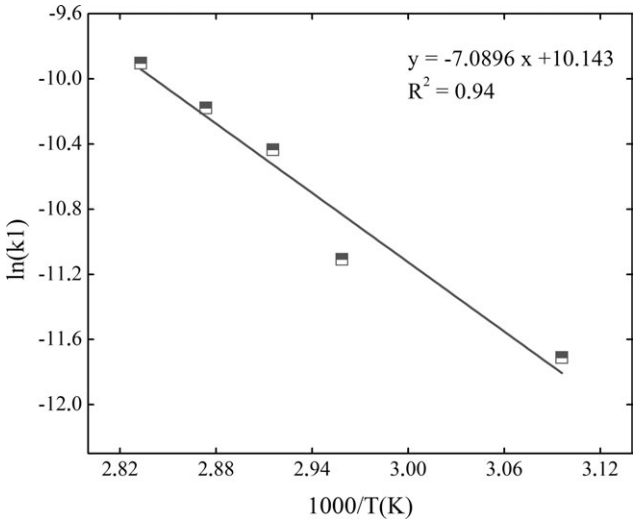

Figure 10. Arrhenius-type plot for reaction constant k_1.

The activation energies estimated from dynamic and isothermal measurements were very similar. They were calculated from dynamic DSC data using the Kissinger (58.87 kJ mol^{-1}) and Ozawa–Flynn–Wall (62.02 kJ mol^{-1}) models, and from isothermal DSC data using the Arrhenius-type dependence of the reaction rate constants, k_1 and k_2, with temperature (58.94 and 45.32 kJ mol^{-1}, respectively). The value of k_2 was found to be higher than the value of k_1 for all temperatures, suggesting that

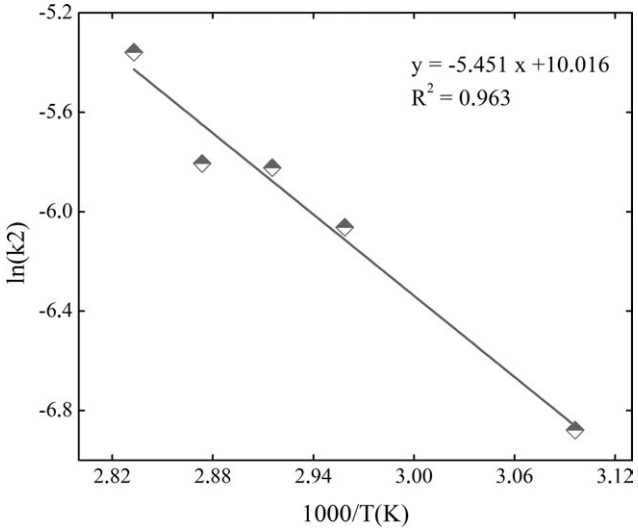

Figure 11. Arrhenius-type plot for reaction constant k_2.

Table VI. k_1 and k_2 Activation Energies and Pre-Exponential Factors for AEHO-Based Resin

E_{a1} (kJ mol^{-1})	E_{a2} (kJ mol^{-1})	A_1	A_2
58.94	45.32	$e^{10.14}$	$e^{10.02}$

the curing behavior of this bioresin is more influenced by autocatalytic mechanisms than by *n*th order mechanisms.

Future Work

The study of the thermo-mechanical properties of 100% biocomposite panels manufactured with the synthesized AEHO bioresin and a reinforcement of natural fiber mats (Jute fiber) will be undertaken and reported. A comparative study of the structural properties of biocomposites prepared with the EHO and the AEHO bioresins will also be reported in the near future.

ACKNOWLEDGMENTS

The authors thank the Queensland State Government for providing a Smart Futures PhD Scholarship, the Australian Government for providing an Endeavor Research Award, and the National Scientific and Technical Research Council of Argentina (CONICET), which provided the financial support for this research work.

REFERENCES

1. Wool, R. P.; Khot, N. *ASM Handbook Comp. (ASM Int.)* **2001,** *21*, 184.
2. Chen, W. Y.; Wang, Y. Z.; Chang, F. C. *J. Appl. Polym. Sci.* **2004,** *92*, 892.
3. Wisanrakkit, G.; Gillham, J. K. *J. Appl. Polym. Sci.* **1990,** *41*, 2885.
4. Ramos, J. A.; Pagani, N.; Riccardi, C. C.; Borrajo, J.; Goyanes, S. N.; Mondragon, I. *Polmag* **2005,** *46*, 3323.
5. Rosu, D.; Mititelu, A.; Cascaval, C. N. *Polym. Test.* **2004,** *23*, 209.
6. Ghaemy, M.; Rostami, A. A.; Omrani, A. *Polym. Int.* **2005,** *55*, 279.
7. Mathew, D.; Reghunadhan Nair, C. P.; Krishnan, K.; Ninan, K. N. *J. Polym. Sci. A Polym. Chem.* **1999,** *37*, 1103.
8. Du, S.; Guo, Z. S.; Zhang, B.; Wu, Z. *POLYIEI* **2003,** *53*, 1343.
9. Ghaemy, M.; Barghamadi, M.; Behmadi, H. *J. Appl. Polym. Sci.* **2004,** *94*, 1049.
10. Vyazovkin, S.; Sbirrazzuoli, N. *Macromolecules* **1996,** *29*, 1867.
11. Ramirez, C.; Rico, M.; Barral, L.; Diez, J.; Garcia-Garabal, S.; Montero, B. *J. Therm. Anal. Calorim.* **2007,** *87*, 69.
12. Vyazovkin, S.; Sbirrazzuoli, N. *Macromol. Chem. Phys.* **1999,** *200*, 2294.
13. Kenny, J. M.; Trivisano, A. *Polym. Eng. Sci.* **1991,** *31*, 1426.
14. Kenny, J. M. *J. Appl. Polym. Sci.* **1994,** *51*, 761.
15. Kissinger, H. E. *Anal. Chem.* **1957,** *29*, 1702.
16. Liang, G.; Chandrashekhara, K. *J. Appl. Polym. Sci.* **2006,** *102*, 3168.
17. Liang, G.; Garg, A.; Chandrashekhara, K.; Flanigan, V.; Kaplia, S. *J. Reinf. Plast. Compos.* **2005,** *24*, 1509.
18. Zhu, J.; Chandrashekhara, K.; Flanigan, V.; Kaplia, S. *J. Appl. Polym. Sci.* **2004,** *91*, 3513.
19. Badrinarayanan, P.; Yongshang, L.; Larock, R. C.; Kessler, M. R. *J. Appl. Polym. Sci.* **2009,** *113*, 1042.
20. Park, S. J.; Jin, F. L.; Lee, J. R. *Macromol. Rapid. Commun.* **2004,** *25*, 724.
21. Martini, D. S.; Braga, B. A.; Samios, D. *Polym.* **2009,** *50*, 2919.
22. Manthey, N. W.; Cardona, F.; Aravinthan, T.; Cooney, T. *J. Appl. Polym. Sci.* **2011,** *122*, 444.
23. Manthey, N. W.; Cardona, F.; Aravinthan, T. J. *Appl. Polym. Sci.* **2012,** *125*, E511.
24. La Scala, J.; Wool, R. P. *Polym.* **2005,** *46*, 61.
25. Malik, M.; Choudhary, V.; Varma, I. K. *Rev. Machromol. Chem. Phys.* **2000,** *C40*, 139.
26. Lem, K. W.; Han, C. D. *Polym. Eng. Sci.* **1984,** *24*, 175.
27. Vilas, J. L.; Laza, J. M.; Garay, M. T., Rodriguez, M.; Leon, L. M. *J. Appl. Polym. Sci.* **2001,** *79*, 447.
28. Horie, K.; Hiura, H.; Sawada, M.; Mita, I.; Kambe, J. *J. Polym. Sci. A-1* **1970,** *8*, 1357.
29. Sourour, S.; Kamal, M. R. *SPE Thermochim. Acta* **1976,** *14*, 41.
30. Kamal, M. R. *Polym. Eng. Sci.* **1974,** *14*, 231.
31. Stevenson, J. F. *Polym. Eng. Sci.* **1986,** *26*, 746.
32. Hale, A.; Makosko, C. W.; Bair, H. E. *Proc ANTEC'87* **1987,** *33*, 1110.
33. Lee, J. H.; Lee, J. W. *Polym. Eng. Sci.* **1994,** *34*, 742.
34. Chern, C. S.; Poehlein, G. W. *Polym. Eng. Sci.* **2004,** *7*, 788.
35. Cole, K. C. *Macromolecules* **1991,** *24*, 3093.
36. Yousefi, A.; Lafleur, P. G. *Polym. Compos.* **1997,** *18*, 157.
37. Peyser, P.; Bascom, W. D. *J. Appl. Polym. Sci.* **1977,** *21*, 2359.
38. Prime, R. B. *Polym. Eng. Sci.* **1973,** *13*, 365.
39. Han, C. D.; Lee, D. S. *J. Appl. Polym. Sci.* **1987,** *34*, 793.
40. Gonzalez-Romero, V. M.; Casillas, N. *Polym. Eng. Sci.* **1989,** *29*, 295.
41. Patel, P. S.; Shah, P. P.; Patel, S. R. *Polym. Eng. Sci.* **1986,** *26*, 1186.
42. Flynn, J. H.; Wall, L. A. *J. Res. Natl. Bur. Stand. Sect. A* **1966,** *42*, 487.
43. Ozawa, T. *J. Therm. Anal. Calorim.* **1970,** *2*, 301.
44. Islam, M. S.; Pickering, K. L.; Foreman, N. J. *J. Adhes. Sci. Technol.* **2009,** *23*, 2085.
45. Dupuy, J.; LeRoy, E.; Maazouz, A. *J. Appl. Polym. Sci.* **2000,** *78*, 2262.
46. Omrani, A.; Simon, L. C.; Rostami, A. A.; Ghaemy, M. *Eur. Polym. J.* **2008,** *44*, 769.
47. Karkanas, P. I.; Partridge I. K. *J. Appl. Polym. Sci.* **2000,** *77*, 1419.
48. Barral, L.; Cano, J.; Lopez, J.; Lopez-Bueno, I.; Nogueira, P.; Abad, J.; Ramirez, C. *J. Polym. Sci. B Polym. Phys.* **1999,** *38*, 351.
49. Lu, M. G.; Shim, M. J.; Kim, S. W. *Appl. Chem.* **1997,** *1*, 357.